Sensitivity study of the residue method for the detection of aerosols from space-borne sensors

Martin de Graaf

April 2002

Sensitivity study of the residue method for the detection of aerosols from space-borne sensors

Contents

Abstract

In this study the residue method (Torres *et al.*, 1998) for the detection of absorbing aerosols from space-borne sensors has been investigated. It uses the spectral variations of the backscattered radiances in the near ultraviolet produced by the interaction between aerosols and molecular scattering to separate aerosol absorption from scattering effects. The departure of the observed spectral contrast from that of a molecular atmosphere is computed. Its dependence on aerosol and environment variables has been investigated with several simulated aerosol laden atmospheres using a radiative transfer model. The residue increases with increasing optical thickness and aerosol layer altitude as expected. This study confirms the capability of the residue method for the detection of elevated absorbing aerosols by space-borne sensors. It can be used as an indicator for aerosol type distinction.

1 Introduction

Aerosols affect the radiation budget of the Earth-atmosphere system directly by the scattering and absorption of solar radiation, and indirectly as cloud condensation nuclei. The large climate modification potential of aerosols has attracted much scientific interest. Satellite-based sensing of aerosols is one of the most used techniques to determine the time and space distribution of aerosols on a global basis. Recent developments make detection of aerosols from satellites possible, but a complete description of the aerosol load in terms of physical quantities is not (yet) possible. Here a technique for the detection of absorbing aerosols, the residue or spectral contrast anomaly method, is subject to a sensitivity analysis. This method separates the spectral contrast caused by absorbing aerosols from that of all other effects, including molecular Rayleigh scattering, surface reflection, gaseous absorption and aerosol and cloud scattering. The residue method has been developed and described by Torres *et al.* (1998) for the TOMS satellite instrument. It can also be applied to UV satellite spectrometers like GOME, SCIAMACHY en OMI. The advantage of the method is that the residue is negative or close to zero for clouds and scattering aerosols, but positive for elevated absorbing aerosols. Therefore it can be used to discriminate between different aerosol types. In the next section the method is described in more detail. After that the results of an extensive sensitivity study are shown and discussed.

1.1 Definition of the residue

The residue r is a wavelength dependent variable defined as

$$r_\lambda = -100 \cdot \left\{ {}^{10}\log(\frac{I_\lambda}{I_{\lambda_0}})_{meas} - {}^{10}\log(\frac{I_\lambda}{I_{\lambda_0}})_{Ray} \right\}, \tag{1}$$

where I_λ is the radiance at the top of the atmosphere (TOA) at a wavelength λ. The subscript $_{meas}$ refers to a measured or simulated real atmosphere TOA radiance, as opposed to a TOA radiance in a Rayleigh atmosphere, where only (multiple) scattering from gases and surface reflection occurs. The latter is referred to as $_{Ray}$. The reflectance is defined as

$$R = \frac{\pi I}{\mu_0 E_0}, \tag{2}$$

where E_0 is the solar irradiation at TOA perpendicular to the direction of the incident sunlight and μ_0 is the cosine of the solar zenith angle θ_0. So $\mu_0 E_0$ is the solar irradiance at TOA incident on a horizontal surface unit.

If the surface albedo for the Rayleigh atmosphere calculation is chosen so that $(I_{\lambda_0})_{meas} = (I_{\lambda_0})_{Ray}$, where λ_0 is some reference wavelength, then equation (1) can be reduced to

$$r_\lambda = -100 \cdot {}^{10}\log\left(\frac{(R_\lambda)_{meas}}{(R_\lambda)_{Ray}}\right), \tag{3}$$

where $(R_\lambda)_{Ray}$ is dependent on the surface albedo. The radiances in equation (1) are replaced by reflectances, because according to equation (2) quotients of radiances are equal to quotients of reflectances.

This quantity emerged as a by-product of ozone detection algorithms for space borne sensors (Herman *et al.*, 1997). For the detection of ozone an accurate separation of the wavelength dependence of backscattered radiation due to ozone absorption and that due to atmospheric scattering is necessary. r was designed as a measure of the error in the ozone algorithm, which in many cases turned out to be caused by UV absorbing aerosols. In this context it is often referred to as the Absorbing Aerosol Index (AAI), e.g. by Hsu *et al.* (1996), Torres *et al.* (2001), Pandithurai *et al.* (2001) and Torres *et al.* (2002). In this study the wavelength for which the residue is calculated is 340 nm, and the reference wavelength λ_0 for which an equivalent surface albedo under a Rayleigh atmosphere is calculated, is 380 nm. At these wavelengths the gaseous (ozone) absorption is weak and backscattered radiation is primarily controlled by Rayleigh scattering, surface reflection and scattering from aerosols and clouds. These wavelengths are also used in other sensitivity studies of the residue method (Herman *et al.*, 1997; Torres *et al.*, 1998).

The residue method is explained in Figure 1. In the top panel an absorbing aerosol case is plotted, while in the lower panel a scattering case is given. Referring to the top panel the dashed-dotted line gives the measured spectral dependence of the reflectance in a real atmosphere with an absorbing aerosol layer between 3 and 4 kilometres. (Actually, this 'measurement' is a radiative transfer model simulation in which the aerosols are modelled with an optical thickness of 1.0, single scattering albedo of 0.7 and a Henyey-Greenstein phase function with an asymmetry parameter of 0.7; the surface albedo is 0.05.) The dashed line gives the reflectance if no aerosols are present (Rayleigh atmosphere) for the same surface albedo. We see that the backscattered radiation is decreased for all wavelengths, due to the absorption by the aerosols. Now the aerosol atmosphere is approximated by a pure Rayleigh atmosphere with a different, but wavelength independent, surface albedo. Using the measured value at 380 nm to fix the Rayleigh case a surface albedo of 0.009 is found. The Rayleigh reflectance for this surface albedo is given by the solid line. We see that a wavelength independent surface albedo does not produce a good approximation for all wavelengths. This is the essence of the residue method, which is a measure of the deviation of both curves at a wavelength other than 380 nm. The case shown here yields a residue r of 3.5 at 340 nm.

The lower panel in Figure 1 shows a similar case, but now for scattering aerosols. The backscattered reflectance is now larger than the backscattered Rayleigh reflectance, giving rise to a higher equivalent surface albedo of 0.16. The Rayleigh curve for this albedo matches the aerosol curve much better, leading to a lower residue. In the case of scattering aerosols the spectral dependence of the residue is opposite to the one of absorbing aerosols, yielding a negative value (in the case shown here the residue is -1 at 340 nm).

1.2 Calculation of the residue

The above section gives the definition of the residue. Here the computational method is described.

Firstly, look-up tables (LUTs) were generated containing TOA Rayleigh atmosphere reflectances at 340 nm and 380 nm versus surface albedo. The geometry of the problem can be defined by three angles: the solar zenith angle θ_0, the viewing zenith angle θ and the azimuth angle $\phi - \phi_0$. For discrete values of the geometry and surface albedo reflectance values were stored in a file. The azimuth angle was equidistantly discretized, for every 10 degrees a value was stored. The viewing and solar zenith angles were discretized using 24 Gaussian points and 8 user-defined, convenient values. The surface albedo range from 0 to 1 was divided into 100 equal intervals. Now, the geometry of the problem is used to find the equivalent Rayleigh reflectance at 380 nm. The nearest available values for the geometry are identified, the corresponding reflectances are read and a three point interpolation is performed in θ_0 and θ and a linear interpolation in $\phi - \phi_0$. This yields the sought equivalent Rayleigh reflectance value for the problem geometry, with a corresponding surface albedo. The 340 nm reflectance at this surface albedo is found in a similar LUT approach.

To examine the residue behaviour for different kinds of atmospheric circumstances and aerosol compositions, a sensitivity study was performed. The next sections discuss the results.

2 Effect of aerosol parameters on residue

In this section the effect of several aerosol parameters on the residue is studied, as well as the effect of the optical thickness of the aerosols and the effect of polarisation.

2.1 Standard aerosol and atmosphere parameters

To check the sensitivity of the residue several parameters are varied in turn relative to a standard case. This standard case represents a cloudless sky with an aerosol layer of one kilometre, the base of which is at 3 km altitude. For the atmospheric gas profile, the standard Mid-Latitude Summer (MLS) atmosphere (Anderson *et al.*, 1986) has

Table [1]: *Aerosol and atmosphere parameters*

parameter			standard	min.	max.
optical thickness	τ	[-]	1	0	4
single scattering albedo	ω_0	[-]	0.9	0.6	1
asymmetry parameter	g	[-]	0.7	0.4	0.85
surface albedo	As	[-]	0.05	0	1
height of the aerosol layer base	z	[km]	3	0	10

been adopted throughout all calculations. The ground pressure is 1013 hPa, the ozone column is 334 DU. The atmosphere is described in terms of a multi-layer plane-parallel atmosphere. The layers can have Rayleigh scattering, gas absorption and aerosol and cloud particle scattering and absorption. Polarisation can be taken into account. The aerosol phase function is approximated with a single Henyey-Greenstein function. The single Henyey-Greenstein function is defined as (Hovenier and Hage, 1989)

$$\Phi(\cos\Theta) = \frac{1-g^2}{(1+g^2-2g\cos\Theta)^{3/2}}. \tag{4}$$

Here, Θ is the scattering angle and $g = <\cos\Theta>$ is the asymmetry parameter. In Figure 14 some examples of single Henyey-Greenstein functions are given. In the standard case an asymmetry parameter of $g = 0.7$ and a single scattering albedo of the aerosols of $\omega_0 = 0.9$ is used. These values are typical for absorbing aerosols (IPCC, 2001). The optical thickness τ of the aerosol layer is 1. The surface albedo A_s is set to 0.05, which is a typical value for both land and sea in UV. In Table [1] the values are summarised and the range of the variation is given. The calculations are performed with the Doubling-Adding KNMI radiative transfer model (DAK) (Stammes, 2001). The doubling-adding method is described by De Haan *et al.* (1987) and Hovenier and Van der Mee (1983). The model computes radiance, polarisation and irradiance at TOA and inside the atmosphere. Plots of residues are presented in the following form: The residue is plotted versus the varied parameter for 5 solar zenith angles: $\theta_0 = 0$, 30, 45, 60 and 75 degrees and nadir view, corresponding to scattering angles of 180, 150, 135, 120 and 105 degrees, respectively. Firstly, a plot is shown with calculations where linear polarisation is taken into account and secondly a plot without polarisation.

2.2 Aerosol optical thickness

Figure 2 shows the dependence of the residue on the optical thickness of the aerosol layer. The residue is zero for zero optical thickness, which is to be expected. Zero optical thickness represents a clear sky which has zero residue by construction. The residue increases with increasing optical thickness. This can be explained as follows. As the optical thickness increases, multiple scattering becomes more important and more background radiation is absorbed and less radiation will emerge at the TOA. Therefore, the deviation from the clear sky radiation increases, yielding a higher residue value. Torres *et al.* (1998) show increasing residues with increasing optical thickness, with slopes proportional to the single scattering albedo for a solar zenith angle of 40°, nadir view, surface albedo of 0.05 and an aerosol layer at 2.9 km altitude. Figure 2 shows that linear dependencies between residue and optical thickness fall apart at optical thicknesses greater than one, or at higher solar zenith angles ($> 60°$). For these cases a higher order approximation seems more appropriate. The residue is dependent on solar zenith angle, because for higher solar zenith angles the optical thickness of the slant atmosphere increases, reducing R both at 340 and 380 nm. Therefore the spectral contrast becomes less pronounced, yielding lower residues. This can be expressed by the

geometrical airmass M, which is defined as

$$M = \frac{1}{\mu_0} + \frac{1}{\mu}. \tag{5}$$

If μ_0 or μ decreases, the geometrical path through the atmosphere increases. In this study μ is one (nadir view), so M increases with decreasing solar zenith angle.

Neglecting polarisation in the radiance calculations yields a divergence of the curves for different θ_0, but the general behaviour of the curves is about the same as in Figure 2a.

2.3 Single scattering albedo

Secondly, the aerosol single scattering albedo is varied between 0.6 and 1, in steps of 0.05. Figure 3 shows the resultant residue. The residue decreases with increasing single scattering albedo as expected: absorbing aerosols should yield positive residues, while scattering aerosols should yield zero or negative residue. The abrupt endings of the plot reveal a restriction of the residue method. In case of highly absorbing aerosols and low surface albedo, the measured/calculated 380 nm radiance is so much reduced by absorbing aerosols, that there may be no equivalent lower surface reflectance under a Rayleigh atmosphere with the same reduced radiances at the TOA. In this case no residue can be found. For absorbing aerosols single scattering albedos are typically 0.8 to 0.9. Torres *et al.* (1998) use 0.65 for highly absorbing aerosols, but the residue for this case with a surface albedo of 0.05 can not be reproduced.

2.4 Asymmetry parameter

The asymmetry parameter of the aerosols is varied in Figure 4. It is a measure for the amount of forward scattered radiance by aerosols; the greater g, the greater the amount of radiance scattered in the forward direction. For Rayleigh scattering the amount of radiation in the forward direction is equal to the amount of backward scattering, so g is zero. Aerosols scatter mainly in the forward direction, thus having positive g values, in the range of $g = 0.40 - 0.85$. In this range, the residue is slightly raised for stronger forward scattering. As the amount of forward scattered radiation increases, more radiation reaches the surface where absorption takes place yielding a higher residue. Also, for higher g the effect of scattering is reduced compared to the effect of absorption, leading to higher residues.

In Figure 5 the same dependence is shown as in Figure 4a, but now the surface albedo is increased. In Figure 5a the surface albedo is 0.6 and the effect of absorption at the surface is reduced and hence the residue is smaller for larger g. Now the effect of a decreasing scaled optical thickness $\tau' = \tau(1 - g)$ with increasing g becomes more important. The amount of exactly forward scattered light increases with increasing g, leading to a decreased scaled aerosol optical thickness and decreased residue. In Figure 5b the effect of absorption at the surface is absent (the surface albedo is 1) and now the residue is almost constant with varying g.

2.5 Polarisation

In the previous figures the results for both polarisation and no polarisation in the calculations are given. In general the curves for different solar zenith angles lie closer together if polarisation is taken into account. Neglecting polarisation gives rise to errors of a few percent in the radiance calculations. A residue of 1.0 means a radiance change of 2.3 percent, so errors of a few percent will yield erroneous residues, but this is limited if the Rayleigh atmosphere reflectances in the look-up table are calculated in the same way as the simulated aerosol atmosphere reflectances. If vector radiances (with polarisation, as occurs in reality) are interpreted as scalar radiances (without polarisation), the resulting apparent residue can be quite large. Using LUTs with scalar radiances, $(I_\lambda)_{Ray}$ and $(I_{\lambda_0})_{Ray}$ in equation (1), and vector radiances for the Rayleigh atmosphere radiances, $(I_\lambda)_{meas}$ and $(I_{\lambda_0})_{meas}$, the residue is not equal to zero as should be in a Rayleigh atmosphere. This is illustrated in Figure 6a: the scalar and vector reflectances at 340 and 380 nm are plotted as function of solar zenith angle. The differences in the reflectances are in the order of 8 % maximum near $\mu_0 = 0.15$ and $\mu_0 = 1$. The apparent residue is plotted in the same figure, and can be as large as ± 4. If scalar radiances are used with vector LUT radiances the sign of the apparent residue is reversed. In Figure 6b the variations of the apparent residue with solar and viewing zenith angle is plotted.

In the further discussions only results will be shown with residues which are calculated with reflectances in which linear polarisation is taken into account.

3 Effect of atmospheric and surface conditions on residue

Next the dependence of the residue on the atmospheric variables and the surface is investigated. The standard aerosols are introduced in the atmosphere, but the conditions of the atmosphere are changed.

3.1 Surface albedo

In Figure 7 the result of a changing surface albedo is plotted. For low surface albedo up till about 0.4 the residue is positive for all solar zenith angles. In general, the residue decreases for higher surface albedos, although this result is strongly dependent on solar zenith angle. For small solar zenith angles the residue is almost constant for increasing surface albedo, while for large solar zenith angles the residue becomes negative, because scattering becomes much more important than the absorption by aerosols.

3.2 Height of the aerosol layer

The residue is highly dependent on the height of the aerosol layer as shown in Figure 8. The value on the x-axis in Figure 8 refers to the base of the one kilometre thick aerosol layer. The dependence is linear in height, and almost the same for all solar zenith angles. This was also found by Torres *et al.* (1998) and Herman *et al.* (1997). The explanation is that absorbing aerosols mainly interact with backscattered radiation,

coming from below. The higher the aerosol layer, the greater the amount of affected molecular radiation. This means that the residue method is especially suited for detection of stratospheric and high tropospheric aerosols. To illustrate this, the residue is also calculated for aerosols located low in the troposphere. An aerosol layer is introduced in the lower kilometre of the atmosphere and the residue is calculated for this case. Figures 9 and 10 show the behaviour of the residue on changing optical thickness and single scattering albedo, respectively. Figure 9 shows that the residue is almost zero for this case, varying between -0.6 and 0.4. An increasing optical thickness does not yield larger residues, which means that even very thick 'clouds' of lower tropospheric aerosols will not be detected. Note that the variation with solar zenith angle is greatest if τ is 1.0, which is a typical value for aerosols.

The aerosol single scattering albedo is varied between 0.4 and 1 in Figure 10. The resultant residue variation is larger this time, between -1 and +1, for large θ_0. Again we see that the residue decreases for increasing single scattering albedo, but the residues are small. Scattering aerosols produce negative residues, as can be seen in both Figures 3 and 10, especially for large solar zenith angles. This is consistent with Torres *et al.* (1998), who found residues of around -1 for large, scattering aerosols. Also, according to Torres *et al.* (1998), observations show that sulfate aerosols do produce negative residues and are located over regions of high industrial activity. Figures 3 and 10 show that this result is not limited to high altitude aerosols if the solar zenith angle is large enough ($> 45°$).

3.3 Clouds

The influence of clouds is shown in Figures 11a and 11b. The cloud is characterised by a high optical thickness of $\tau = 50$, an asymmetry parameter $g = 0.85$ and a single scattering albedo $\omega_0 = 1$. The vertical extent of the cloud is 1 km. The left side of Figure 11a shows the residue when the cloud is placed under the aerosol layer, which has an altitude of $3 - 4$ km. The residue is the same as for an aerosol layer over a bright surface (compare the left side of Figure 11a with Figure 7a with a high surface albedo). The cloud reflects almost all light incident on it, so effectively this becomes the new surface. As the cloud base is raised the residue is slightly reduced, due to a decrease in amount of intercepted radiation by the aerosol layer (the distance between the cloud and the aerosol layer is reduced). Then there is a transition to a new situation, where the cloud overlies the aerosol layer. The residue drops by about 1 in the new situation and stays almost constant when the cloud is raised. The cloud intercepts almost all incident radiation, and acts as an opaque 'roof' over the aerosol layer. The same is valid for Figure 11b, where the aerosol layer is between 0 and 1 kilometre. Here the residue is almost entirely determined by the cloud characteristics. The cloud is a scattering aerosol and produces zero or negative residues, depending on the solar zenith angle.

Table [2]: *Optical properties of the aerosol models used in Figure 12.*

Aerosol Model	ω_0	g
S1	1.00	0.73
S2	1.00	0.70
C1	0.93	0.71
C2	0.85	0.73
D1	0.91	0.67
D2	0.74	0.79
D3	0.65	0.86

4 Effect of residue for different aerosol types

In the previous sections we used a theoretical phase function, described by a single Henyey-Greenstein function with $g = 0.7$ and $\omega_0 = 0.9$, sometimes varied within the range applicable to aerosols to study the residue behaviour. Now we turn to more realistic aerosol phase functions, to describe more realistically the aerosols found in the earth's atmosphere. First we use Henyey-Greenstein functions again, but now with more specific values for g and ω_0 and then we use Mie theory to describe the aerosol phase functions.

4.1 Henyey-Greenstein phase functions

Seven types of aerosols were defined and their effect on the residue was determined under several atmospheric conditions. The seven aerosol types are constructed to be close to the aerosol types defined by Torres *et al.* (1998). Here the aerosols are characterised using a single Henyey-Greenstein phase function, whereas Torres *et al.* (1998) use Mie calculations to determine the scattering properties of the particles. The single scattering albedos and asymmetry parameters of the types used in this study are listed in Table [2]. The types S1 and S2 represent scattering aerosols such as sea salt and stratospheric sulfuric acid aerosols. Types C1 and C2 are weakly and moderately absorbing carbonaceous aerosols, respectively, representative of old and fresh smoke particles. Types D1 to D3 are increasingly stronger absorbing aerosols, representative of increasingly larger mineral aerosols like desert dust. In Figure 12 the residues are plotted as a function of aerosol optical thickness for an aerosol layer between 3 and 4 km altitude, over a surface with albedo 0.05 (a) and 0.6 (b), for a solar zenith angle of 40° and nadir view. These curves show the same behaviour as those for the aerosol models used by Torres *et al.* (1998). Large, highly absorbing aerosols (C2, D2 and D3) produce positive residues that increase with optical thickness. Smaller, weakly absorbing aerosols produce significantly lower residues (C1 and D1), while scattering aerosols produce negative residues (S1 and S2). The curves deviate slightly from the ones of Torres *et al.* (1998). First of all, the curve for D3 is not complete. For small surface albedo the residues produced by the very

strongly absorbing aerosols can not be calculated. Extrapolating the curve to an optical thickness $\tau = 1$ would yield the same residue that Torres *et al.* (1998) find, but in our case this would require negative surface albedo values, or otherwise reduced reflectance values. Secondly, the types S1 and S2 cannot be discriminated. Torres *et al.* (1998) find lower S1 residues than S2 residues, but here they are about the same.

In Figure 12b the effect of a high surface albedo is given. The residue is lower because of the contribution of the surface reflection to the TOA radiance, but absorbing aerosols are still detectable. The residue for type D3 can now be produced for the entire optical thickness interval, because the surface albedo is very large, so smaller reflectance values can easily be found. The most conspicuous deviation from the study of Torres *et al.* (1998) is the larger spreading of the C2, D2 and D3 type curves in Figure 12 for an optical thickness $\tau = 1$. According to the study of Torres *et al.* (1998) these curves are almost indiscriminable, whereas Figure 12 shows quite clear deviations at $\tau = 1$. Also the residue is lower for types C1 and D1 and also for S1 and S2 than found by Torres *et al.* (1998), but the general behaviour matches quite well, even though we use Henyey-Greenstein functions to describe the phase functions.

4.2 Mie phase functions

The aerosol size distribution parameters and refractive indices mentioned by Torres *et al.* (1998) were used in Mie calculations to compute the optical properties of the seven aerosol types mentioned above. In Table [3] the particle size distribution parameters of the Mie calculations are given, as well as the optical properties at the wavelengths 340 nm and 380 nm. The form of the assumed particle size distribution is a log-normal function. Figure 15 shows the phase functions of the different aerosol types at 380 nm in the backscatter range. Figure 13 shows the residues of a layer of Mie aerosols between 3 and 4 kilometre altitude, surface albedo 0.05 (a) and 0.6 (b), solar zenith angle 40° and nadir view. As in Figure 12, the residue for the highly absorbing aerosol type D3 can not be reproduced at low surface albedo. In general, the residues found with Mie phase functions are higher than those found with Henyey-Greenstein phase functions. For scattering aerosols the residues are the same for Mie and Henyey-Greenstein phase functions. Comparing Figure 13 with Torres *et al.* (1998) we see a good comparison. Only the residues produced by the aerosol types S1 and S2 can not be discriminated in Figure 13a, contrary to what Torres *et al.* (1998) find. Again, for high surface albedos the residues for C2, D2 and D3 lie further apart than in the study of Torres *et al.* (1998). Also the residues found here are higher than presented by Torres *et al.* (1998). The main differences of the results in this study and the one of Torres *et al.* (1998), are probably caused by the different vertical distributions of both studies. In (Torres *et al.*, 1998) the vertical distribution of the aerosols is represented by a Gaussian profile with a maximum at 3 km and a width of 1 km. In this study the aerosol layer is homogeneous and between 3 and 4 km altitude.

Table [3]: *Particle size distributions parameters of the aerosol models used in Figure 13 and their optical properties at two wavelengths.*

Aerosol			Refractive	340		380	
Model	$r_0(\mu)$	σ	Index	ω_0	g	ω_0	g
S1	0.07	2.03	1.43 - 0.000i	1.00	0.73	1.00	0.73
S2	0.40	1.43	1.43 - 0.000i	1.00	0.70	1.00	0.70
C1	0.14	1.45	1.55 - 0.020i	0.90	0.71	0.90	0.71
C2	0.14	1.45	1.55 - 0.040i	0.82	0.73	0.83	0.73
D1	0.07	1.95	1.57 - 0.015i	0.90	0.68	0.91	0.67
D2	0.25	2.20	1.57 - 0.015i	0.72	0.80	0.73	0.78
D3	0.50	2.20	1.57 - 0.015i	0.63	0.87	0.65	0.86

5 Errors

The residue calculations are subject to errors because of the interpolations of LUT values. Here an estimate of these errors is given.

As outlined in section 1.2, reflectance values are stored for discrete values of μ_0, μ and $\phi - \phi_0$. The intervals of $\phi - \phi_0$ are equidistant, but μ_0 and μ are divided by 24 Gaussian points plus eight user-defined values. The maximum distance between tabulated points of μ_0 and μ is 0.042, for angles of around 47° and 71°. The maximum error introduced by linearly interpolating the LUT values was estimated by calculating the residue for a geometry which needed interpolation over the largest intervals and comparing it with a direct, 'exact' computation of the residue. This revealed errors in the residue of less than 0.1 %. The results in this study have no interpolation errors, except Figures 12 and 13, because they were calculated at tabulated points. An easy estimate of the error in the residue can be obtained by running the program with zero aerosol optical thickness. This yields absolute residues in the order of 10^{-4}, caused by the interpolation errors. In the error calculations the 380 nm reflectances of the aerosol-laden atmosphere and subsequently the surface albedos are also interpolated, but now the surface albedo was divided in equidistant intervals of 0.001 and the relationship between surface albedo and 380 nm TOA reflectances is very smooth. Neglecting polarisation in the reflectance calculations produces errors of a few percent in the reflectance and absolute errors in the residue of 0.5 - 1. This means that polarisation should always be accounted for in the radiance calculations.

6 Conclusions

The general behaviour of the residue as given by Torres *et al.* (1998) and Herman *et al.* (1997) is reproduced in this study. The residue increases with increasing optical

thickness of the aerosol layer and increasing altitude of the layer. This is the basis for the detection of high altitude absorbing aerosols. Also the zero to negative residues for scattering aerosols and clouds is found. The finding that overlying clouds can obscure underlying aerosols is confirmed here.

The most conspicuous aspect of the residue not mentioned by other workers is its dependence on solar zenith and viewing zenith angle, although the smallest variations with solar zenith angle for nadir view are found for an aerosol optical thickness of around one and single scattering albedos of around 0.87, which are typical values for aerosols. But especially for high surface albedos the solar zenith angle plays an important role in the determination of the residue. This is important in high latitude regions, where surface albedos can be very large, also in the UV, because of the presence of snow and ice, and where solar zenith angles are often large. The detection of high altitude absorbing aerosols can be underestimated here compared to other regions. Also for aerosol layers close to the surface the solar zenith angle is of more importance in residue calculations. Variations in aerosol optical thickness and single scattering albedo become more dependent on solar zenith angle for low altitude aerosol layers, especially for optical thicknesses typical for aerosols, both for low and high surface albedos. This means that low clouds can have an important impact on residue calculations. When sub pixel clouds underlie an absorbing aerosol layer the residue of the cloud itself may be zero, but as the cloud will act as the new surface, the residue will become highly dependent on solar zenith angle, especially when the distance between the cloud and the aerosol layer decreases.

The relation between optical thickness and residue is not linear, as Figure 2a shows. Torres *et al.* (1998) and Herman *et al.* (1997) both reported a linear relationship with the slope being proportional to the single scattering co-albedo $(1 - \omega_0)$ of the aerosols. Figures 2, 12 and 13 show that a more accurate approximation would at least have to be of 2^{nd} order.

A weak point of the residue method is the assumed grayness of the surface albedo. In the UV the variation of the surface albedo with wavelength is much less than in the visible range, but it is probably not zero. Herman and Celarier (1997) estimate the difference in surface reflectivity at 340 nm and 380 nm to be 0.2 % maximum. Inclusion of a spectral surface albedo in the residue method would require a cloud fraction retrieval, which is beyond the scope of the AAI algorithm.

Concluding, the AAI algorithm can be a very useful tool for the detection of elevated absorbing aerosols. It can be used to discriminate between absorbing and scattering aerosols. Because it uses UV measurements, the algorithm can be used over oceans as well as terrestrial surfaces, including deserts. It can not be used over high latitude snow and ice covered regions. For absorbing aerosols the residue is very sensitive to the height of the aerosol layer. For high surface albedos, for scattering aerosols or in the presence of subpixel clouds, the result is highly dependent on solar zenith angle. The residue method can not discriminate between different types of absorbing aerosols.

References

Anderson, G. P., S. A. Clough, F. X. Kneizys, J. H. Chetwynd and E. P. Shettle (1986). AFGL atmospheric constituent profiles. Technical Report AFGL-TR-86-0110, Air Force Geophysics Laboratory.

De Haan, J. F., P. B. Bosma and J. W. Hovenier (1987). The adding method for multiple scattering calculations of polarized light. *Astronomy and Astrophysics 183*, 371–391.

Herman, J. R., P. K. Bhartia, O. Torres, C. Hsu, C. Seftor and E. A. Celarier (1997). Global distributions of UV-absorbing aerosols from NIMBUS 7/TOMS data. *Journal of Geophysical Research 102*(D14), 16,911–16,922.

Herman, J. R. and E. A. Celarier (1997). Earth surface reflectivity climatology at 340-380 nm from TOMS data. *Journal of Geophysical Research 102*, 28,003–28,011.

Hovenier, J. W. and J. I. Hage (1989). Relations involving the spherical albedo and other photometric quantities of planets with atmospheres. *Astronomy and Astrophysics 214*, 391–401.

Hovenier, J. W. and C. V. M. van der Mee (1983). Fundamental relationships relevant to the tranfer of polarized light in a scattering atmosphere. *Astronomy and Astrophysics 128*, 1–16.

Hsu, N. C., J. R. Herman, P. K. Bhartia, C. J. Seftor, O. Torres, A. M. Thompson, J. F. Gleason, T. Y. F. Eck and B. N. Holben (1996). Detection of biomass burning smoke from TOMS measurements. *Geophysical Research Letters 23*(7), 745–748.

IPCC (2001). *Working Group I to the Third Assessment Report of the Intergovernmental Panel on Climate Change*. Cambridge Univ. Press, Cambridge, p. 295.

Pandithurai, G., R. T. Pinker, O. Dubovik and T. O. Aro (2001). Remote sensing of aerosol optical characteristics in sub-Sahel, West Africa. *Journal of Geophysical Research 106*(D22), 28,347–28,356.

Stammes, P. (2001). Spectral radiance modelling in the UV-visible range. In W. Smith and Y. Timofeyev (Eds.), *IRS 2000: Current problems in atmospheric radiation*, pp. 385–388. A. Deepak Publishing, Hampton (VA).

Torres, O., P. K. Bhartia, J. R. Herman, Z. Ahmad and J. Gleason (1998). Derivation of aerosol properties from satellite measurements of backscattered ultraviolet radiation: Theoretical basis. *Journal of Geophysical Research 103*(D14), 17,099–17,110.

Torres, O., P. K. Bhartia, J. R. Herman, A. Sinyuk, P. Ginoux and B. Holben (2002). A long-term record of aerosol optical depth from TOMS observations and comparison to AERONET measurements. *Journal of the Atmospheric Sciences 59*(3), 398–413.

Torres, O., R. Decae, P. Veefkind and G. de Leeuw (2001). OMI Aerosol Retrieval Algorithm. In *OMI-EOS Algorithm Theoretical Basis Document, Chapter 4*, pp. 1–24.

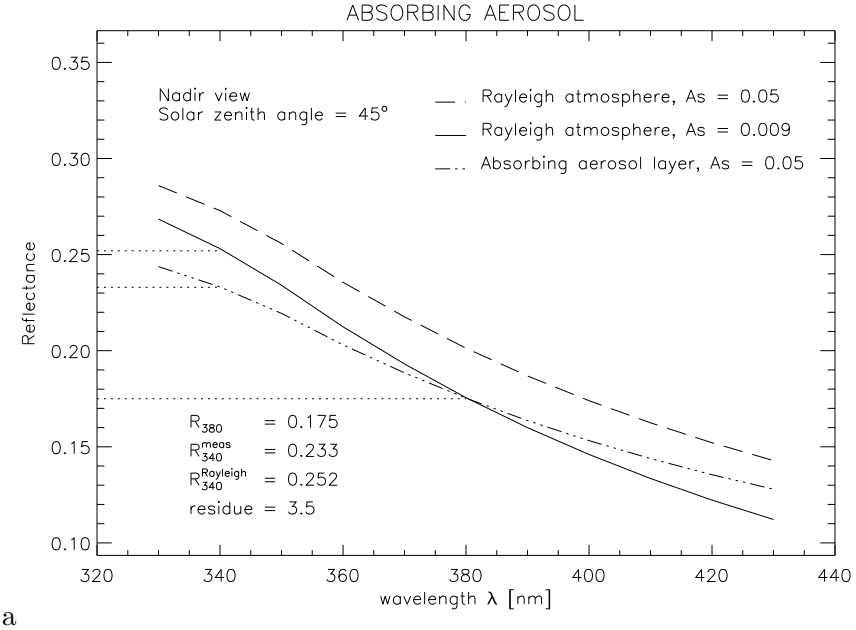

a

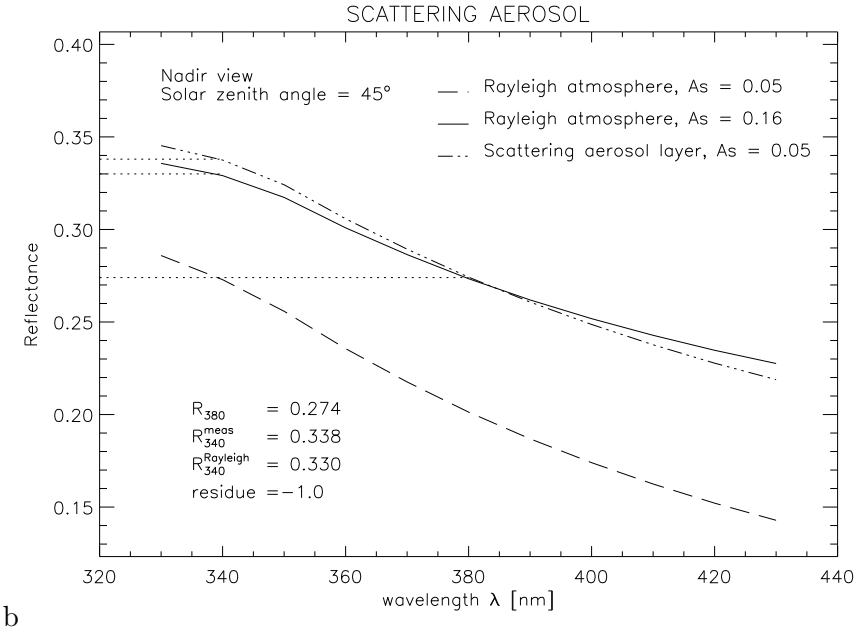

b

Figure 1: *Calculation of the residue. The measured reflectance for an atmosphere with aerosols at 340 and 380 nm are given. From a look-up table of Rayleigh atmosphere reflectances at 380 nm versus surface albedo the latter value is sought. This Rayleigh atmosphere reflectance value is found at a specific surface albedo and with this albedo, the Rayleigh atmosphere reflectance at 340 nm is calculated. These four reflectances together determine the residue. Two examples are given: (a) Absorbing aerosols. (b) Scattering aerosols. See text in section 1.1 for explanation.*

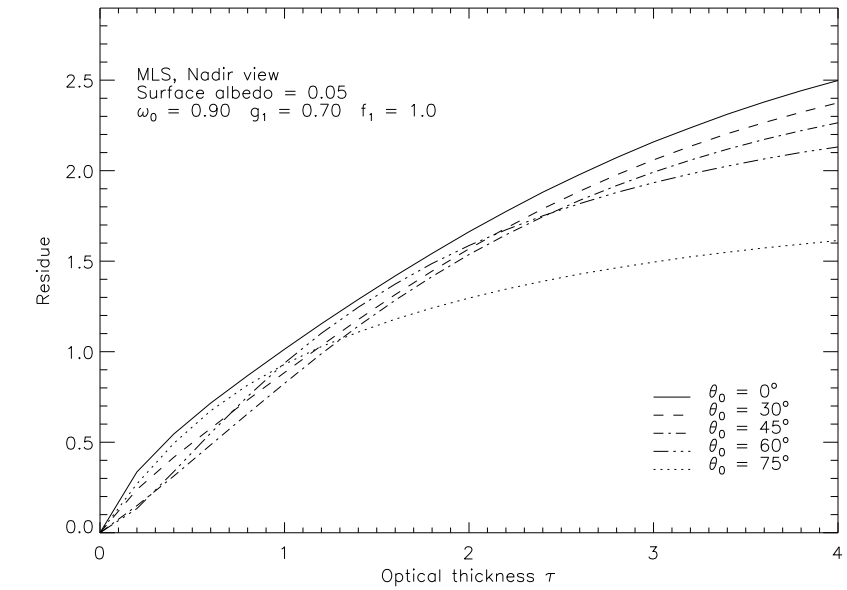

a

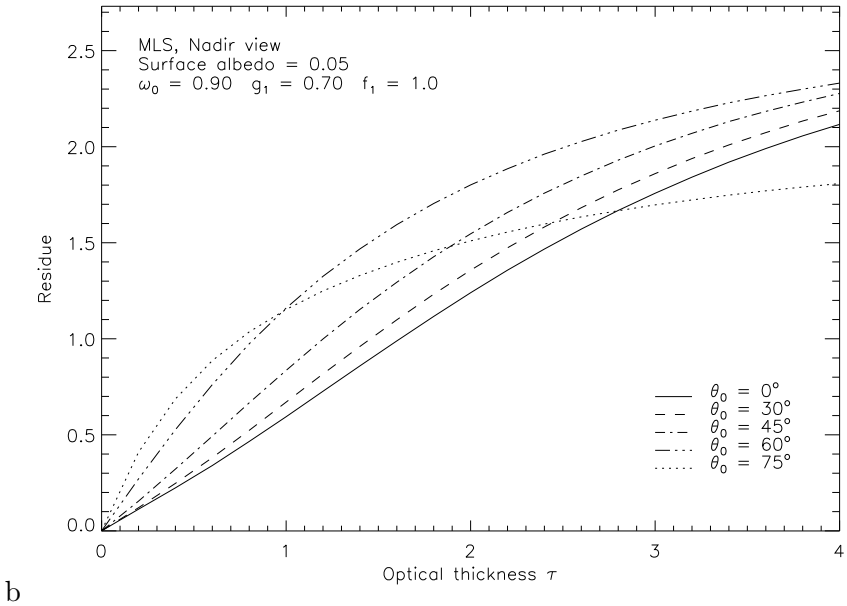

b

Figure 2: *Dependence of the residue on aerosol optical thickness for several solar zenith angles in nadir view. (a) With linear polarisation taken into account in the radiance calculations, (b) without polarisation.*

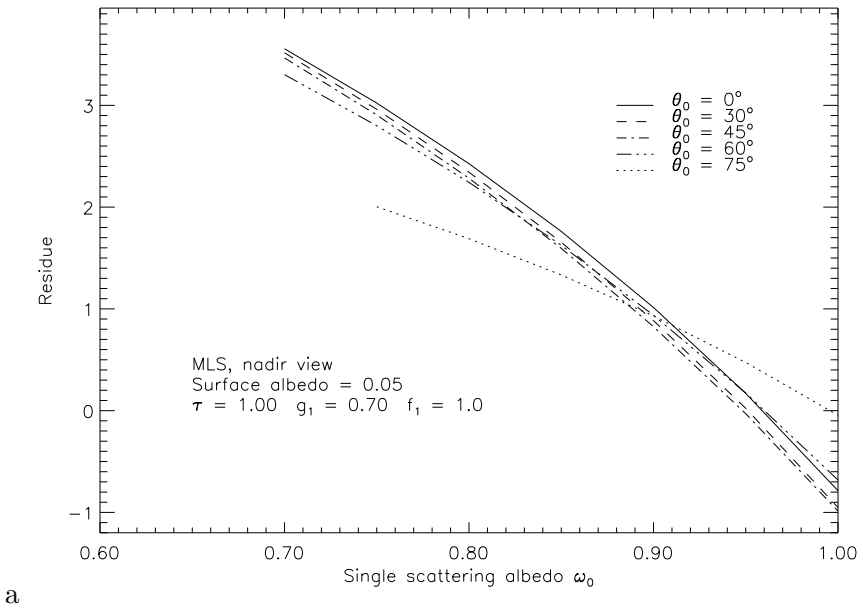

a

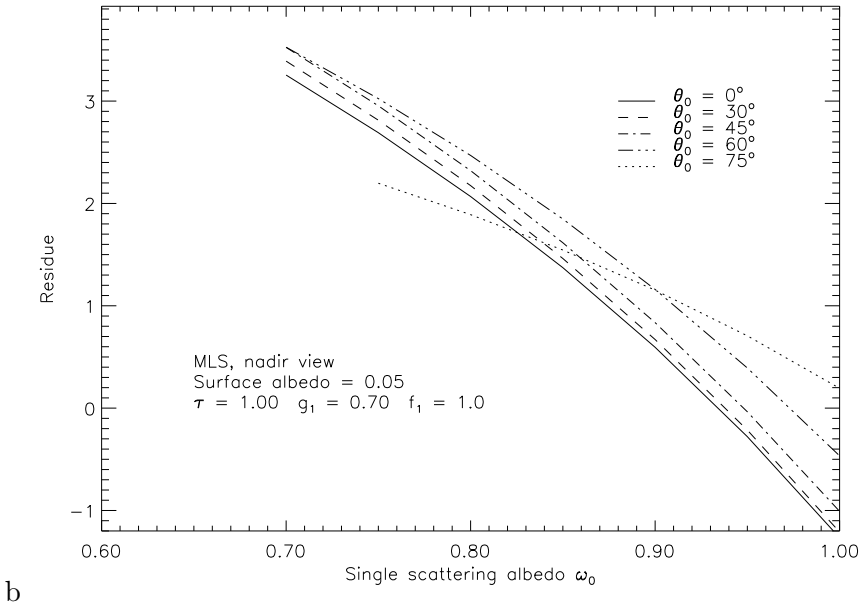

b

Figure 3: *Dependence of the residue on aerosol single scattering albedo for several solar zenith angles in nadir view. (a) With linear polarisation taken into account in the radiance calculations, (b) without polarisation.*

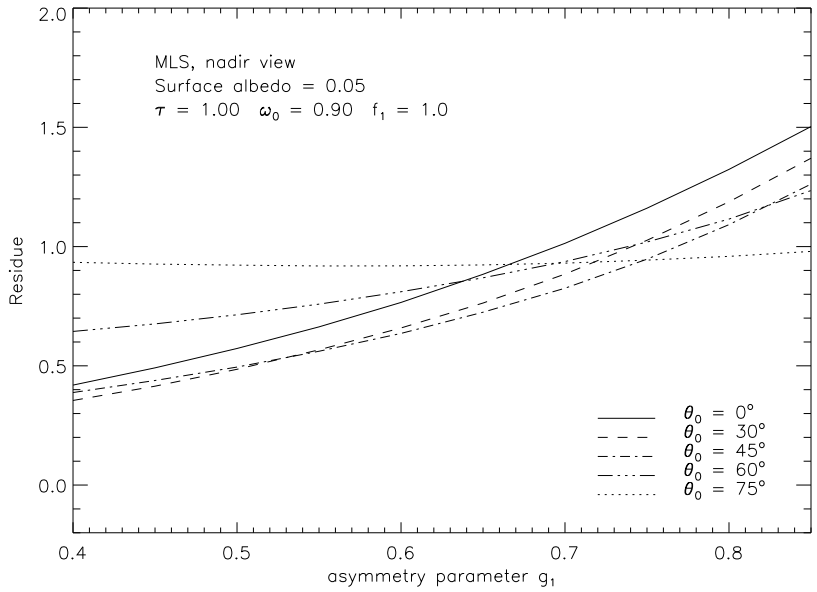

a

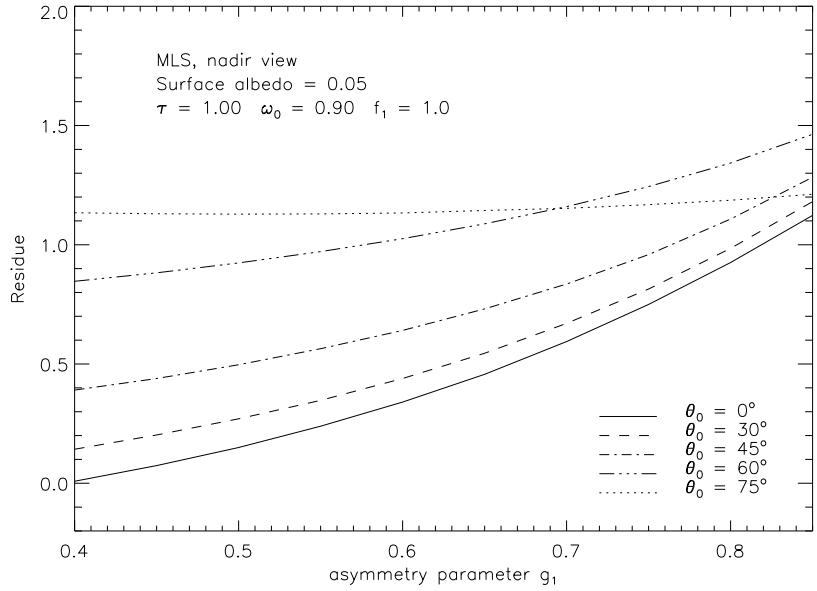

b

Figure 4: *Dependence of the residue on the aerosol asymmetry parameter for several solar zenith angles in nadir view. (a) With linear polarisation taken into account in the radiance calculations, (b) without polarisation.*

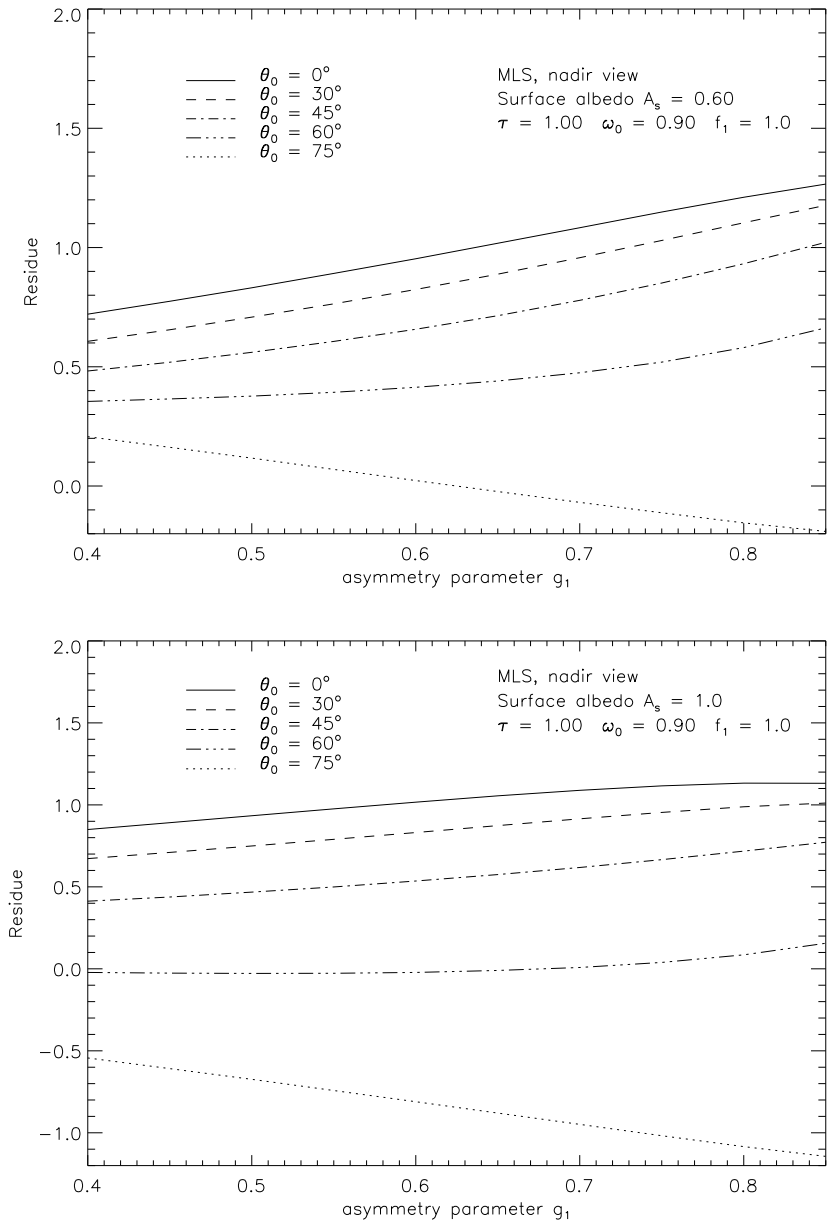

Figure 5: *Dependence of the residue on the aerosol asymmetry parameter for several solar zenith angles in nadir view for high surface albedo. (a) $A_s = 0.6$. (b) $A_s = 1.0$. Linear polarisation is taken into account in the radiance calculations.*

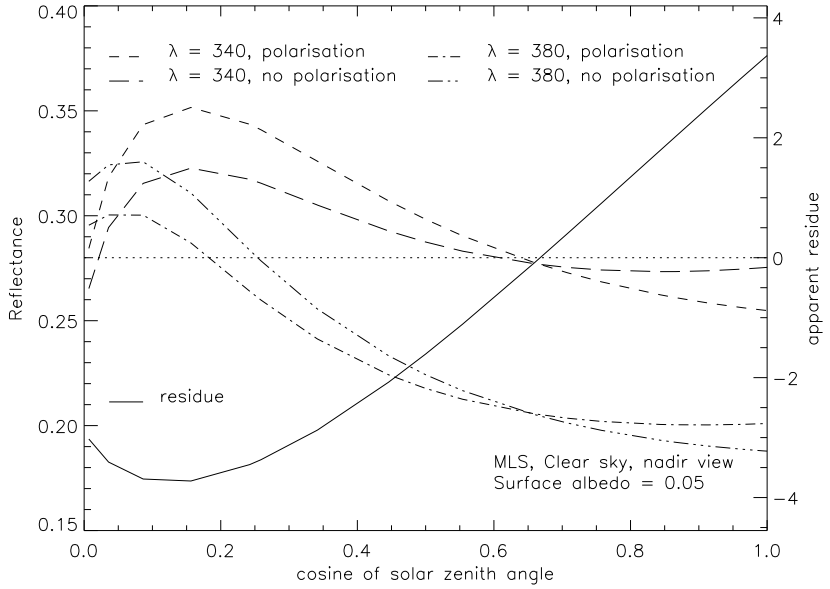

a

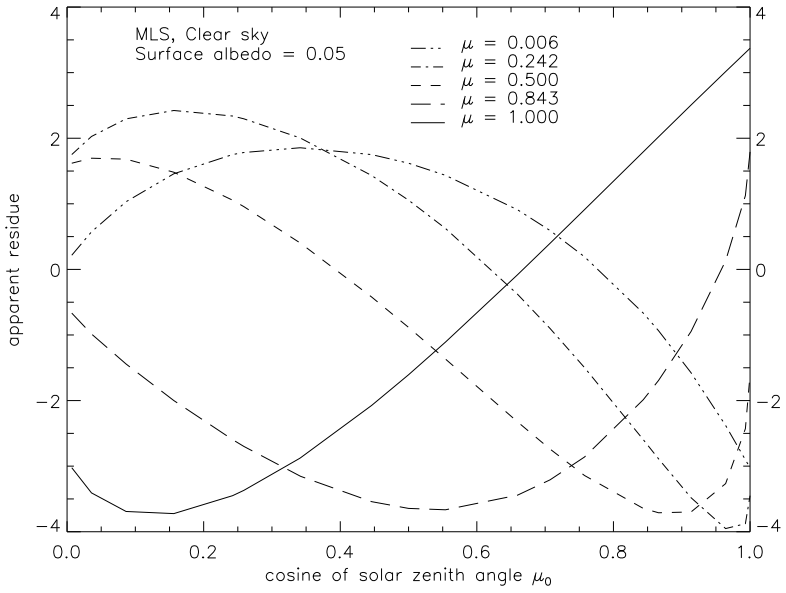

b

Figure 6: *Effect of polarisation in residue calculations: comparing clear sky scalar reflectances with vector reflectances yields non-zero residues. (a) Scalar and vector reflectances at 340 and 380 nm and the corresponding apparent residue in nadir view as a function of solar zenith angle. The surface albedo is 0.05. (b) Dependence of the apparent residue on viewing zenith angle.*

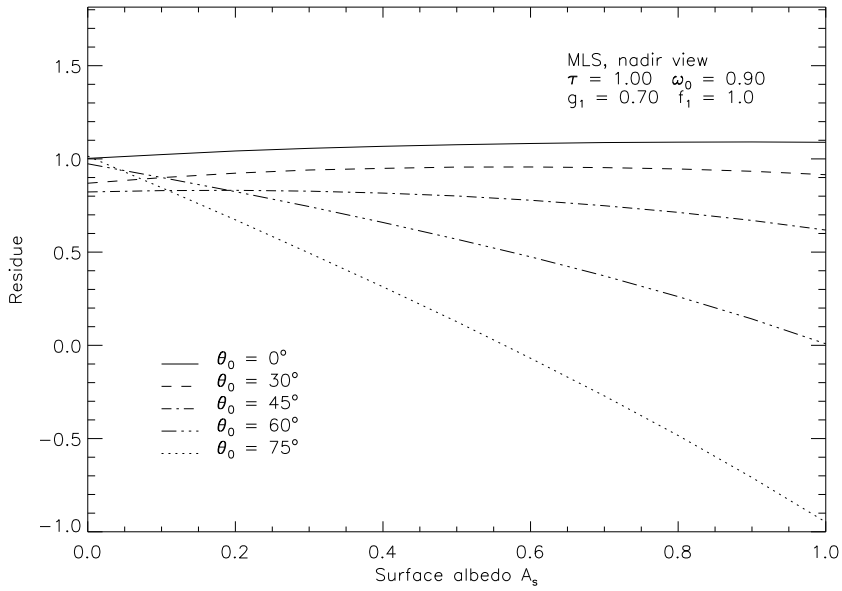

Figure 7: *Dependence of residue on surface albedo.*

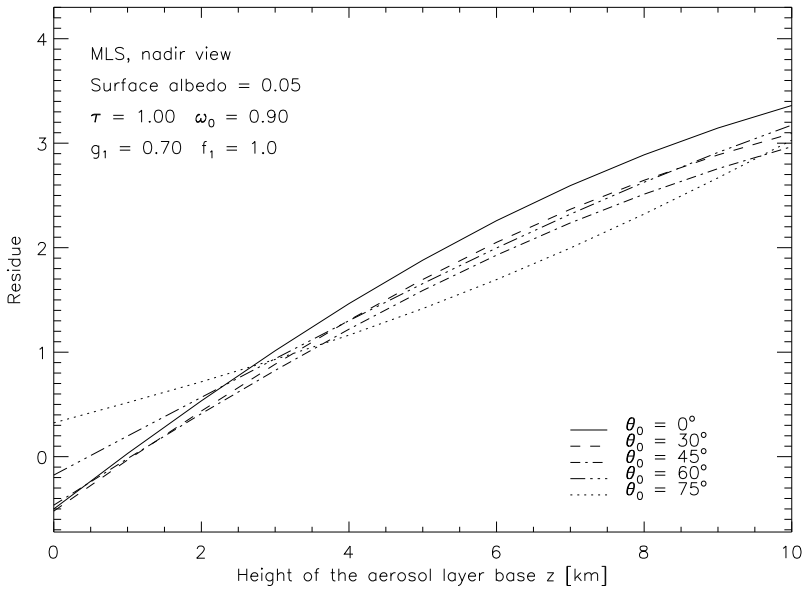

Figure 8: *Dependence of the residue on the base height of the aerosol layer for several solar zenith angles in nadir view. The thickness of the aerosol layer is 1 km.*

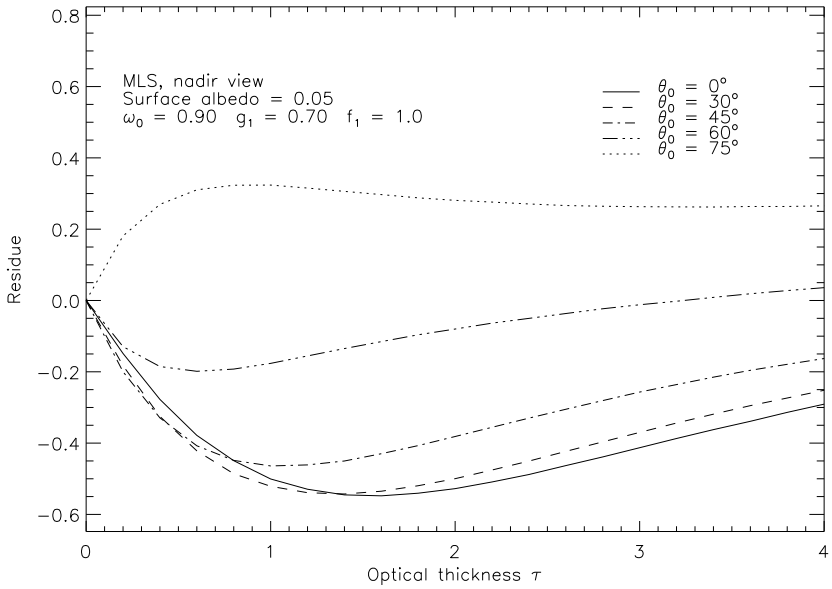

a

Figure 9: *Dependence of the residue on aerosol optical thickness for several solar zenith angles in nadir view with the aerosol layer between 0 and 1 km altitude.*

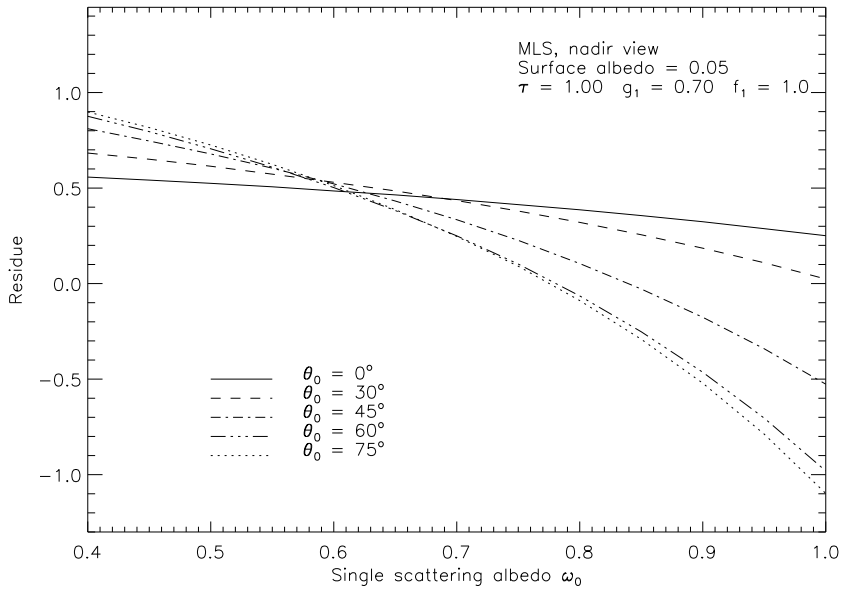

Figure 10: *Dependence of the residue on aerosol single scattering albedo for several solar zenith angles in nadir view with the aerosol layer between 0 and 1 km altitude.*

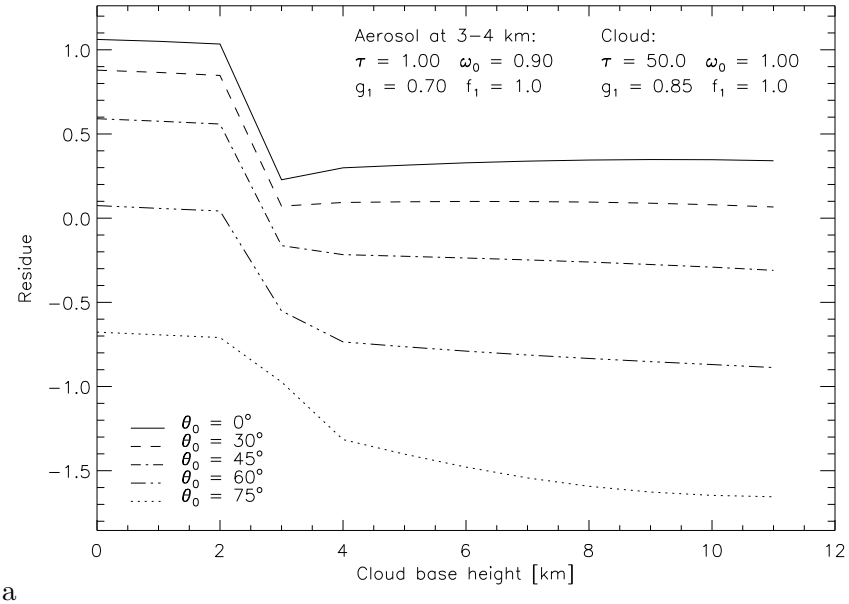

a

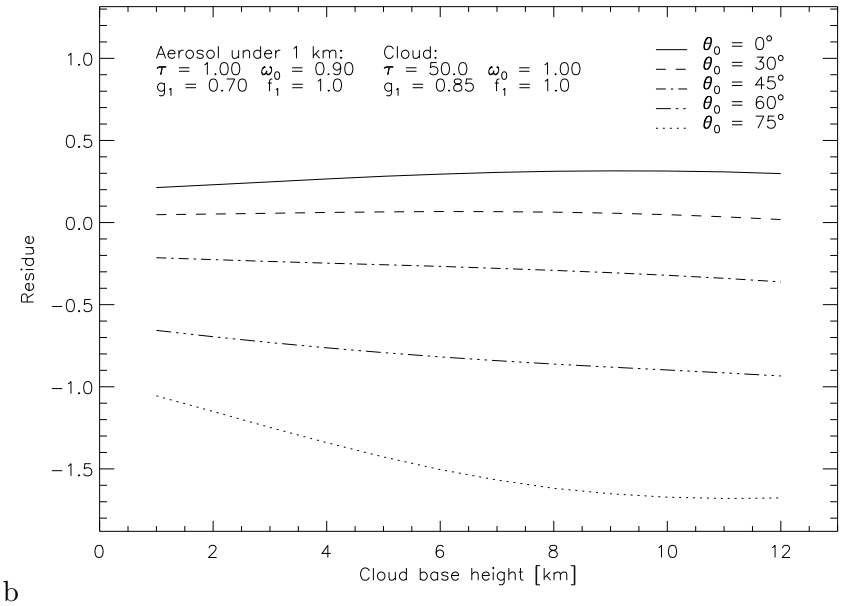

b

Figure 11: *(a) Residue calculations with an aerosol layer between 3 and 4 km altitude and varying cloud base height. With aerosols overlying the cloud, the residue is the same as found with a bright surface (compare with Figure 7). When on the other hand the cloud overlies the aerosol layer, the residue is almost completely determined by the cloud (compare with (b)). (b) Residue calculations with an aerosol layer between 0 and 1 km altitude and varying cloud base height. The residue is almost entirely determined by the cloud characteristics, as most light is reflected by the cloud and almost none absorbed by the aerosols.*

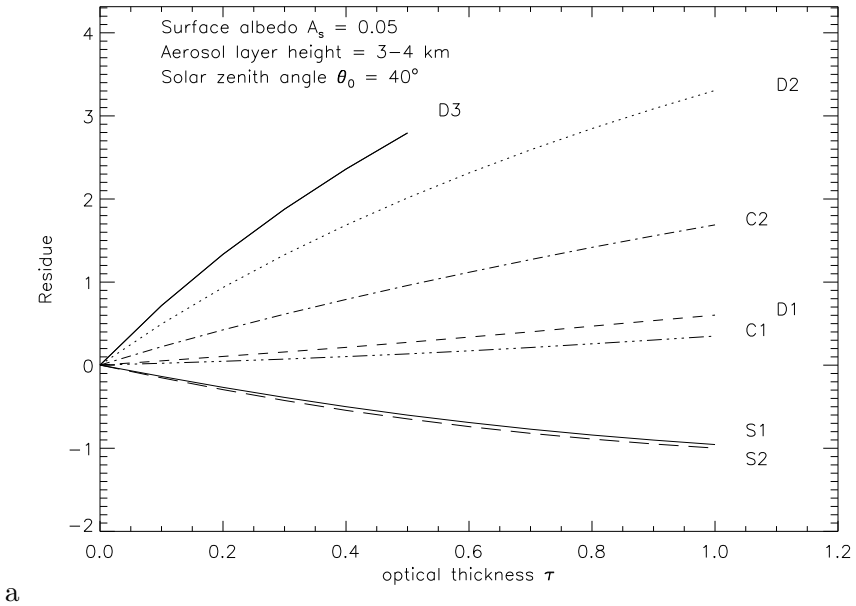

a

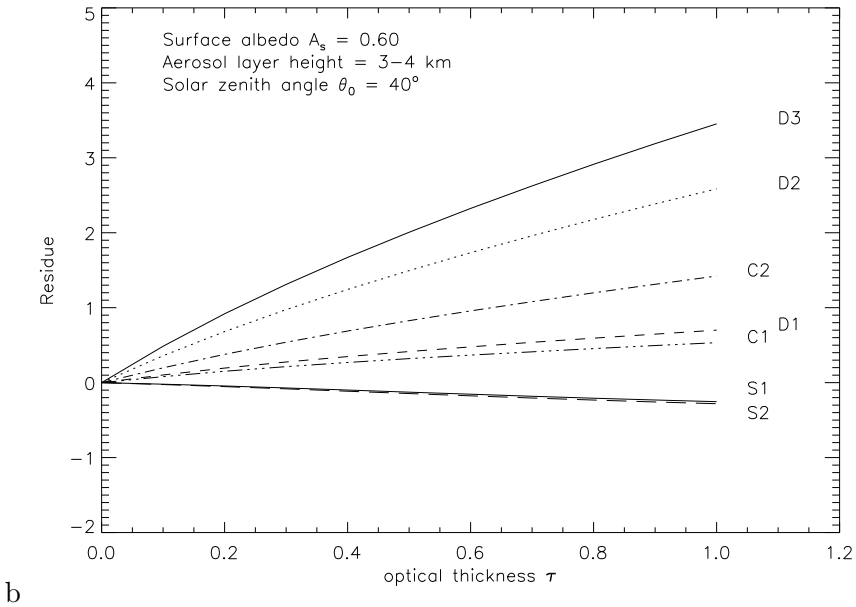

b

Figure 12: *(a) Relationship between the residue and the optical thickness for 7 aerosol types modelled with Henyey-Greenstein phase functions. Conditions are: solar zenith angle 40°, nadir view, surface albedo 0.05 and aerosol layer height 3-4 km. (b) As in (a), but now for surface albedo 0.6.*

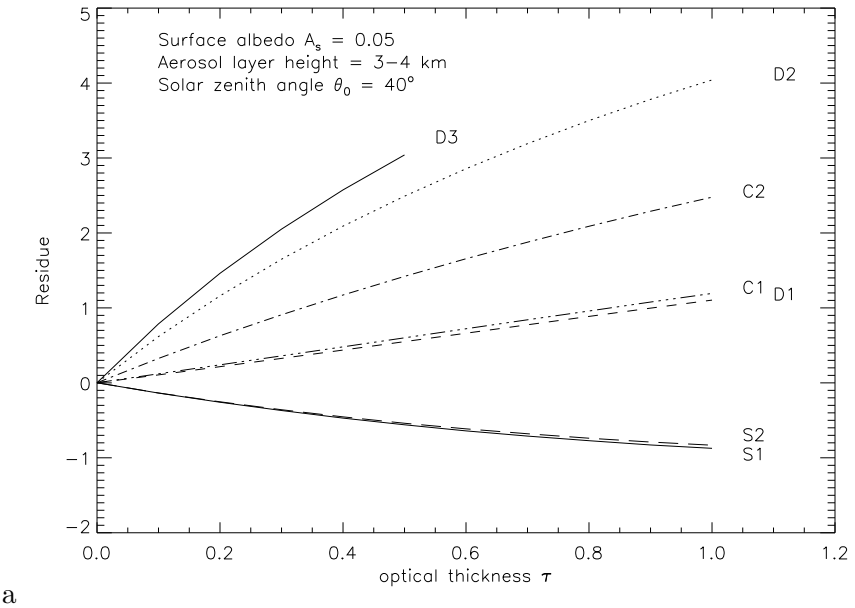

a

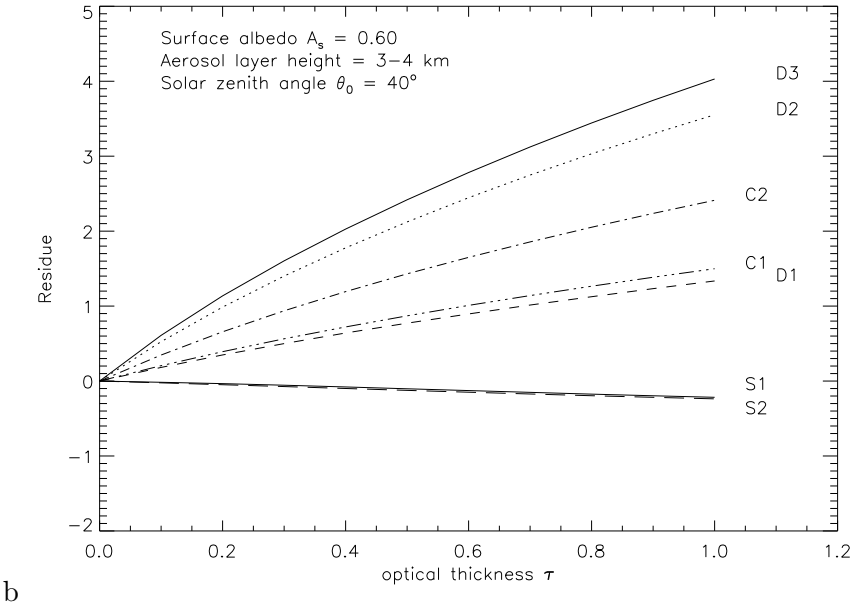

b

Figure 13: *(a) Relationship between the residue and the optical thickness for 7 Mie aerosol types. Conditions are solar zenith angle 40°, nadir view, surface albedo 0.05 and aerosol layer height 3-4 km. (b) As in (a), but now for surface albedo 0.6.*

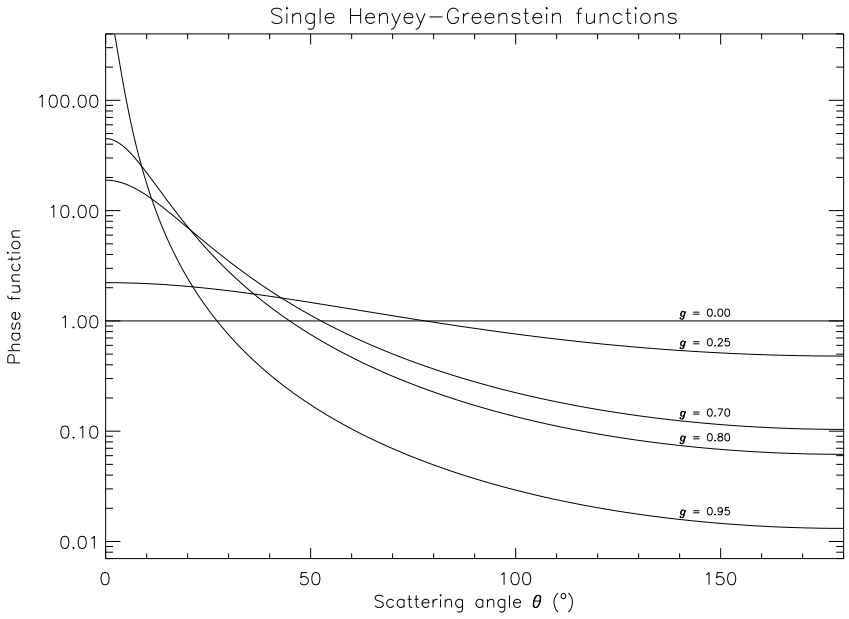

Figure 14: *Single Henyey-Greenstein (HG) phase functions for several different asymmetry parameters g. The aerosol types used in this study are all in the range of* $g = 0.7 - 0.8$*, except D3, which has an asymmetry parameter of 0.86, see table [2]. Note that all single HG functions are monotonically decreasing.*

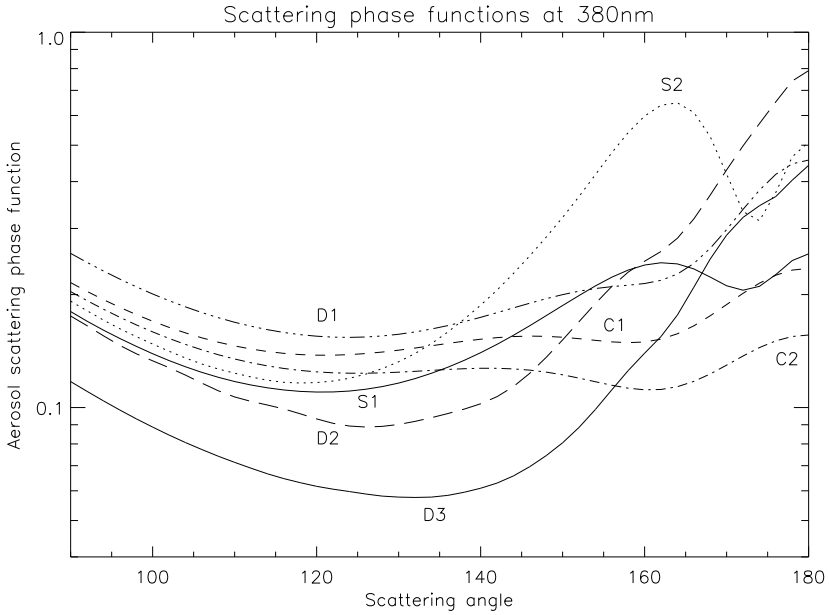

Figure 15: *Mie scattering phase functions at 380 nm for the aerosol types in table [3] in the range of scattering angles relevant to satellite remote sensing.*